*Measurement of polarization amplitudes and CP asymmetries in B[superscript 0] → #K[superscript *](892)[superscript 0]*

Published for SISSA by Springer

Received: *March 13, 2014*
Accepted: *April 17, 2014*
Published: *May 16, 2014*

Measurement of polarization amplitudes and CP asymmetries in $B^0 \to \phi K^*(892)^0$

The LHCb collaboration

E-mail: dlambert@cern.ch

Abstract: An angular analysis of the decay $B^0 \to \phi K^*(892)^0$ is reported based on a pp collision data sample, corresponding to an integrated luminosity of $1.0\,\text{fb}^{-1}$, collected at a centre-of-mass energy of $\sqrt{s} = 7\,\text{TeV}$ with the LHCb detector. The P-wave amplitudes and phases are measured with a greater precision than by previous experiments, and confirm about equal amounts of longitudinal and transverse polarization. The S-wave $K^+\pi^-$ and K^+K^- contributions are taken into account and found to be significant. A comparison of the $B^0 \to \phi K^*(892)^0$ and $\overline{B}^0 \to \phi \overline{K}^*(892)^0$ results shows no evidence for direct CP violation in the rate asymmetry, in the triple-product asymmetries or in the polarization amplitudes and phases.

Keywords: CP violation, Hadron-Hadron Scattering, Polarization, B physics, Flavour Changing Neutral Currents

ArXiv ePrint: 1403.2888

doi:10.1007/JHEP05(2014)069

JHEP05(2014)069

Contents

JHEP05(2014)069

1 Introduction

The decay $B^0 \to \phi K^{*0}$,[1] has a branching fraction of $(9.8 \pm 0.6) \times 10^{-6}$ [1]. In the Standard Model it proceeds mainly via the gluonic penguin diagram shown in figure 1. Studies of observables related to *CP* violation in this decay probe contributions from physics beyond the Standard Model in the penguin loop [2–4]. The decay was first observed by the CLEO collaboration [5]. Subsequently, branching fraction measurements and angular analyses have been reported by the BaBar and Belle collaborations [6–11].

The decay involves a spin-0 B-meson decaying into two spin-1 vector mesons ($B \to VV$). Due to angular momentum conservation there are only three independent configurations of the final-state spin vectors, a longitudinal component where in the B^0 rest frame both resonances are polarized in their direction of motion, and two transverse components with collinear and orthogonal polarizations. Angular analyses have shown that the longitudinal and transverse components in this decay have roughly equal amplitudes. Similar

[1] In this paper K^{*0} is defined as $K^*(892)^0$ unless otherwise stated.

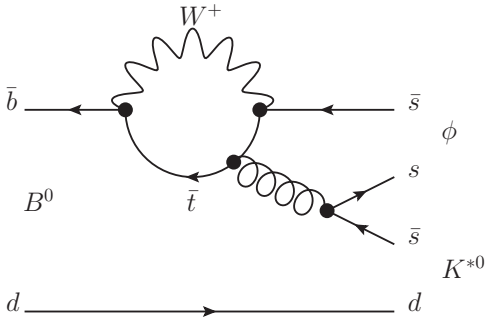

Figure 1. Leading Feynman diagram for the $B^0 \to \phi K^{*0}$ decay.

results are seen in other $B \to VV$ penguin transitions [12–15]. This is in contrast to tree-level decays such as $B^0 \to \rho^+\rho^-$, where the $V-A$ nature of the weak interaction causes the longitudinal component to dominate. The different behaviour of tree and penguin decays has attracted much theoretical attention, with several explanations proposed such as large contributions from penguin annihilation effects [16] or final-state interactions [17, 18]. More recent calculations based on QCD factorization [19, 20] are consistent with the data, although with significant uncertainties.

In this paper, measurements of the polarization amplitudes, phases, *CP* asymmetries and triple-product asymmetries are presented. In the Standard Model the *CP* and triple-product asymmetries are expected to be small and were found to be consistent with zero by previous experiments [6–10]. The studies reported here are performed using *pp* collision data, corresponding to an integrated luminosity of 1.0 fb^{-1}, collected at a centre-of-mass energy of $\sqrt{s} = 7$ TeV with the LHCb detector.

2 Analysis strategy

In this analysis the $B^0 \to \phi K^{*0}$ decay is studied, where the ϕ and K^{*0} mesons decay to K^+K^- and $K^+\pi^-$, respectively (the study of the charge conjugate $\overline{B}^0$ mode is implicitly assumed in this paper). Angular momentum conservation, for this pseudoscalar to vector-vector transition, allows three possible helicity configurations of the vector-meson pair, with amplitudes denoted H_{+1}, H_{-1} and H_0. These can be written as a longitudinal polarization, A_0, and two transverse polarizations, $A_\perp$ and $A_\parallel$,

$$A_0 = H_0 \,, \qquad A_\perp = \frac{H_{+1} - H_{-1}}{\sqrt{2}} \qquad \text{and} \qquad A_\parallel = \frac{H_{+1} + H_{-1}}{\sqrt{2}} \,. \tag{2.1}$$

In addition to the dominant vector-vector (P-wave) amplitudes, there are contributions where either the K^+K^- or $K^+\pi^-$ pairs are produced in a spin-0 (S-wave) state. These amplitudes are denoted $A_{\rm S}^{KK}$ and $A_{\rm S}^{K\pi}$, respectively. Only the relative phases of the amplitudes are physical observables. A phase convention is chosen such that A_0 is real. The remaining amplitudes have magnitudes and relative phases defined as

$$A_\parallel = |A_\parallel| e^{i\delta_\parallel} \,, \; A_\perp = |A_\perp| e^{i\delta_\perp} \,, \; A_{\rm S}^{K\pi} = |A_{\rm S}^{K\pi}| e^{i\delta_{\rm S}^{K\pi}} \text{ and } A_{\rm S}^{KK} = |A_{\rm S}^{KK}| e^{i\delta_{\rm S}^{KK}} \,. \tag{2.2}$$

JHEP05(2014)069

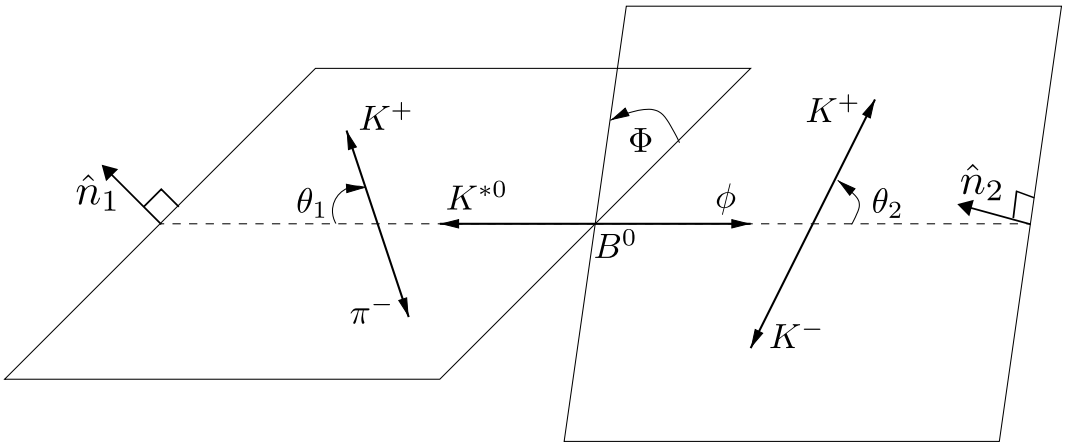

Figure 2. The helicity angles θ_1, θ_2, Φ for the $B^0 \to \phi K^{*0}$ decay.

To determine these quantities, an analysis of the angular distributions and invariant masses of the decay products is performed. It is assumed that the contribution from $B^0 \to K^+K^-K^+\pi^-$, where both the K^+K^- and $K^+\pi^-$ are non-resonant, is negligible.

In the following sections the key elements of the analysis are discussed. First, the conventions used in the angular analysis are defined together with the form of the differential cross-section. Next, the parameterization of the $K^+\pi^-$ and K^+K^- mass distributions is discussed. Finally, the triple-product asymmetries that can be derived from the angular variables are defined.

2.1 Angular analysis

The angular analysis is performed in terms of three helicity angles $(\theta_1, \theta_2, \Phi)$, as depicted in figure 2. The angle θ_1 is defined as the angle between the K^+ direction and the reverse of the B^0 direction in the K^{*0} rest frame. Similarly, θ_2 is the angle between the K^+ direction and the reverse of the B^0 direction in the ϕ rest frame. The angle Φ is the angle between the decay planes of the ϕ and K^{*0} mesons in the B^0 rest frame.

The flavour of the decaying B^0 meson is determined by the charge of the kaon from the K^{*0} decay. To determine the polarization amplitudes, the B^0 and $\overline{B}^0$ decays are combined. For the study of CP asymmetries, the B^0 and $\overline{B}^0$ decays are separated.

Taking into account both the P- and S-wave contributions and their interference, the differential decay rate [8] is given by the sum of the fifteen terms given in table 1,

$$d^5\Gamma = \frac{9}{8\pi} \sum_{i=1}^{15} h_i \; f_i(\theta_1, \theta_2, \Phi) \mathcal{M}_i(m_{K\pi}, m_{KK}) d\Omega(KKK\pi) \; . \tag{2.3}$$

The h_i factors are combinations of the amplitudes, f_i are functions of the helicity angles, $\mathcal{M}_i$ are functions of the invariant mass of the intermediate resonances and $d\Omega(KKK\pi)$ is a four-body phase-space factor,

$$d\Omega(KKK\pi) \propto q_\phi q_{K^*} q_{B^0} \, dm_{K\pi} \, dm_{KK} \, d\cos\theta_1 \, d\cos\theta_2 \, d\Phi \; , \tag{2.4}$$

JHEP05(2014)069

i	h_i	$f_i(\theta_1,\theta_2,\Phi)$	$\mathcal{M}_i(m_{K\pi},m_{KK})$
1	$\lvert A_0\rvert^2$	$\cos\theta_1^2\cos\theta_2^2$	$\lvert M_1^{K\pi}(m_{K\pi})\rvert^2\lvert M_1^{KK}(m_{KK})\rvert^2$
2	$\lvert A_\parallel\rvert^2$	$\frac{1}{4}\sin\theta_1^2\sin\theta_2^2(1+\cos(2\Phi))$	$\lvert M_1^{K\pi}(m_{K\pi})\rvert^2\lvert M_1^{KK}(m_{KK})\rvert^2$
3	$\lvert A_\perp\rvert^2$	$\frac{1}{4}\sin\theta_1^2\sin\theta_2^2(1-\cos(2\Phi))$	$\lvert M_1^{K\pi}(m_{K\pi})\rvert^2\lvert M_1^{KK}(m_{KK})\rvert^2$
4	$\lvert A_\perp\rvert\lvert A_\parallel^*\rvert e^{i(\delta_\perp-\delta_\parallel)}$	$-\frac{1}{2}\sin\theta_1^2\sin\theta_2^2\sin(2\Phi)$	$\lvert M_1^{K\pi}(m_{K\pi})\rvert^2\lvert M_1^{KK}(m_{KK})\rvert^2$
5	$\lvert A_\parallel\rvert\lvert A_0^*\rvert e^{i\delta_\parallel}$	$\sqrt{2}\cos\theta_1\sin\theta_1\cos\theta_2\sin\theta_2\cos\Phi$	$\lvert M_1^{K\pi}(m_{K\pi})\rvert^2\lvert M_1^{KK}(m_{KK})\rvert^2$
6	$\lvert A_\perp\rvert\lvert A_0^*\rvert e^{i\delta_\perp}$	$-\sqrt{2}\cos\theta_1\sin\theta_1\cos\theta_2\sin\theta_2\sin\Phi$	$\lvert M_1^{K\pi}(m_{K\pi})\rvert^2\lvert M_1^{KK}(m_{KK})\rvert^2$
7	$\lvert A_{\rm S}^{K\pi}\rvert^2$	$\frac{1}{3}\cos\theta_2^2$	$\lvert M_0^{K\pi}(m_{K\pi})\rvert^2\lvert M_1^{KK}(m_{KK})\rvert^2$
8	$\lvert A_\parallel\rvert\lvert A_{\rm S}^{*K\pi}\rvert e^{i(\delta_\parallel-\delta_{\rm S}^{K\pi})}$	$\frac{\sqrt{6}}{3}\sin\theta_1\cos\theta_2\sin\theta_2\cos\Phi$	$\lvert M_1^{KK}(m_{KK})\rvert^2 M_1^{K\pi}(m_{K\pi})M_0^{*K\pi}(m_{K\pi})$
9	$\lvert A_\perp\rvert\lvert A_{\rm S}^{*K\pi}\rvert e^{i(\delta_\perp-\delta_{\rm S}^{K\pi})}$	$-\frac{\sqrt{6}}{3}\sin\theta_1\cos\theta_2\sin\theta_2\sin\Phi$	$\lvert M_1^{KK}(m_{KK})\rvert^2 M_1^{K\pi}(m_{K\pi})M_0^{*K\pi}(m_{K\pi})$
10	$\lvert A_0\rvert\lvert A_{\rm S}^{*K\pi}\rvert e^{-i\delta_{\rm S}^{K\pi}}$	$\frac{2}{\sqrt{3}}\cos\theta_1\cos\theta_2^2$	$\lvert M_1^{KK}(m_{KK})\rvert^2 M_1^{K\pi}(m_{K\pi})M_0^{*K\pi}(m_{K\pi})$
11	$\lvert A_{\rm S}^{KK}\rvert^2$	$\frac{1}{3}\cos\theta_1^2$	$\lvert M_0^{KK}(m_{KK})\rvert^2\lvert M_1^{K\pi}(m_{K\pi})\rvert^2$
12	$\lvert A_\parallel\rvert\lvert A_{\rm S}^{*KK}\rvert e^{i(\delta_\parallel-\delta_{\rm S}^{KK})}$	$\frac{\sqrt{6}}{3}\sin\theta_1\cos\theta_1\sin\theta_2\cos\Phi$	$\lvert M_1^{K\pi}(m_{K\pi})\rvert^2 M_1^{KK}(m_{KK})M_0^{*KK}(m_{KK})$
13	$\lvert A_\perp\rvert\lvert A_{\rm S}^{*KK}\rvert e^{i(\delta_\perp-\delta_{\rm S}^{KK})}$	$-\frac{\sqrt{6}}{3}\sin\theta_1\cos\theta_1\sin\theta_2\sin\Phi$	$\lvert M_1^{K\pi}(m_{K\pi})\rvert^2 M_1^{KK}(m_{KK})M_0^{*KK}(m_{KK})$
14	$\lvert A_0\rvert\lvert A_{\rm S}^{*KK}\rvert e^{-i\delta_{\rm S}^{KK}}$	$\frac{2}{\sqrt{3}}\cos\theta_1^2\cos\theta_2$	$\lvert M_1^{K\pi}(m_{K\pi})\rvert^2 M_1^{KK}(m_{KK})M_0^{*KK}(m_{KK})$
15	$\lvert A_{\rm S}^{K\pi}\rvert\lvert A_{\rm S}^{*KK}\rvert e^{i(\delta_{\rm S}^{K\pi}-\delta_{\rm S}^{KK})}$	$\frac{2}{3}\cos\theta_1\cos\theta_2$	$M_1^{KK}(m_{KK})M_0^{K\pi}(m_{K\pi})M_0^{*KK}(m_{KK})M_1^{*K\pi}(m_{K\pi})$

Table 1. Definition of the h_i, f_i and $\mathcal{M}_i$ terms in eq. (2.3). Note that the P-wave interference terms $i=4$ and $i=6$ take the imaginary parts of $A_\perp A_\parallel^*$ and $A_\perp A_0^*$, while $i=5$ takes the real part of $A_\parallel A_0^*$. Similarly the S-wave interference terms $i=9$ and $i=13$ take the imaginary parts of $A_\perp A_{\rm S}^* M_1 M_0^*$, and the terms $i=8,10,12,14$ take the real parts of $A_\parallel A_{\rm S}^* M_1 M_0^*$ and $A_0 A_{\rm S}^* M_1 M_0^*$.

where q_A is the momentum of the daughter particles in the mother's ($A = B^0, \phi, K^{*0}$) centre-of-mass system.

The differential decay rate for $\overline{B}^0 \to \phi\overline{K}^{*0}$ is obtained by defining the angles using the charge conjugate final-state particles and multiplying the interference terms f_4, f_6, f_9, f_{13} by -1. To allow for direct CP violation, the amplitudes A_j are replaced by $\overline{A}_j$, for $j = 0, \parallel, \perp, {\rm S}$. The rate is normalized separately for the $\overline{B}^0$ and B^0 decays such that the P- and S-wave fractions are

$$F_{\rm P} = |A_0|^2 + |A_\parallel|^2 + |A_\perp|^2 \,, \qquad F_{\rm S} = |A_{\rm S}^{K\pi}|^2 + |A_{\rm S}^{KK}|^2 \,, \qquad F_{\rm P} + F_{\rm S} = 1 \,, \tag{2.5}$$

and

$$\overline{F}_{\rm P} = |\overline{A}_0|^2 + |\overline{A}_\parallel|^2 + |\overline{A}_\perp|^2 \,, \qquad \overline{F}_{\rm S} = |\overline{A}_{\rm S}^{K\pi}|^2 + |\overline{A}_{\rm S}^{KK}|^2 \,, \qquad \overline{F}_{\rm P} + \overline{F}_{\rm S} = 1 \,. \tag{2.6}$$

In addition, a convention is adopted such that the phases $\delta_{\rm S}^{K\pi}$ and $\delta_{\rm S}^{KK}$ are defined as the difference between the P- and S-wave phases at the K^{*0} and ϕ meson poles, respectively.

2.2 Mass distributions

The differential decay width depends on the invariant masses of the $K^+\pi^-$ and K^+K^- systems, denoted $m_{K\pi}$ and m_{KK}, respectively. The P-wave $K^+\pi^-$ amplitude is parameterized using a relativistic spin-1 Breit-Wigner resonance function,

$$M_1^{K\pi}(m_{K\pi}) = \frac{m_{K\pi}}{q_{K^*}} \frac{m_0^{K^*}\Gamma_1^{K\pi}(m_{K\pi})}{(m_0^{K^*})^2 - m_{K\pi}^2 - i m_0^{K^*}\Gamma_1^{K\pi}(m_{K\pi})} \,, \tag{2.7}$$

JHEP05(2014)069

where $m_0^{K^*} = 895.81$ MeV/c^2 [1] is the K^{*0} mass. The mass-dependent width is given by

$$\Gamma_1^{K\pi}(m_{K\pi}) = \Gamma_0^{K^*} \frac{m_0^{K^*}}{m_{K\pi}} \frac{1 + r^2 q_0^2}{1 + r^2 q_{K^*}^2} \left(\frac{q_{K^*}}{q_0} \right)^3 , \tag{2.8}$$

where q_0 is the value of q_{K^*} at $m_0^{K^*}$, $r = 3.4\ \hbar c/\text{GeV}$ [21] is the interaction radius and $\Gamma_0^{K^*} = 47.4\,\text{MeV}/c^2$ is the natural width of the K^{*0} meson [1]. The P-wave K^+K^- amplitude, denoted $M_1^{KK}(m_{KK})$, is modelled in a similar way using the values $m_0^{\phi} = 1019.455$ MeV/c^2 and $\Gamma_0^{\phi} = 4.26$ MeV/c^2 [1]. In the case of the ϕ meson the natural width is comparable to the detector resolution of 1.2 MeV/c^2, which is accounted for by convolving the Breit-Wigner with a Gaussian function.

As the K^{*0} is a relatively broad resonance, the S-wave component in the $K^+\pi^-$ system, denoted $M_0^{K\pi}(m_{K\pi})$, needs careful treatment. In this analysis the approach described in ref. [8] is followed, which makes use of the LASS parameterization [21]. This takes into account an $L = 0$ $K_0^*(1430)$ contribution together with a non-resonant amplitude. The values used for the LASS parameterization are taken from ref. [8].

Finally, an S-wave in the K^+K^- system is considered. This is described by the Flatté parameterization of the $f_0(980)$ resonance [22],

$$M_0^{KK}(m_{KK}) = \frac{1}{m_{f_0}^2 - m_{KK}^2 - i m_{f_0}(g_{\pi\pi}\rho_{\pi\pi} + g_{KK}\rho_{KK})} , \tag{2.9}$$

where the $g_{KK,\pi\pi}$ are partial decay widths and the $\rho_{KK,\pi\pi}$ are phase-space factors. The values $m_{f_0} = 939\,\text{MeV}/c^2$, $g_{\pi\pi} = 199\,\text{MeV}/c^2$ and $g_{KK}/g_{\pi\pi} = 3.0$ were measured in ref. [23]. The Flatté distribution is convolved with a Gaussian function to account for the detector resolution. Other approaches to modelling the mass distributions for both the $K^+\pi^-$ and K^+K^- S-wave are considered as part of the systematic uncertainty determination.

2.3 Triple-product asymmetries

The amplitudes and phases can be used to calculate triple-product asymmetries [2, 4, 24]. Non-zero triple-product asymmetries arise either due to a T-violating phase or a CP-conserving phase and final-state interactions. Assuming CPT symmetry, a T-violating phase, which is a *true* asymmetry, implies that CP is violated.

For the P-wave decay, two triple-product asymmetries are calculated from the results of the angular analysis [4],

$$A_T^1 = \frac{\Gamma(s_{\theta_1\theta_2} \sin\Phi > 0) - \Gamma(s_{\theta_1\theta_2} \sin\Phi < 0)}{\Gamma(s_{\theta_1\theta_2} \sin\Phi > 0) + \Gamma(s_{\theta_1\theta_2} \sin\Phi < 0)} \quad \text{and} \quad A_T^2 = \frac{\Gamma(\sin 2\Phi > 0) - \Gamma(\sin 2\Phi < 0)}{\Gamma(\sin 2\Phi > 0) + \Gamma(\sin 2\Phi < 0)} , \tag{2.10}$$

where $s_{\theta_1\theta_2} = \text{sign}(\cos\theta_1 \cos\theta_2)$. These asymmetries can be rewritten in terms of the interference terms between the amplitudes [4], h_4 and h_6 in table 1,

$$A_T^1 = -\frac{4}{\pi}\mathcal{I}m(A_\perp A_0^*) \qquad \text{and} \qquad A_T^2 = -\frac{2\sqrt{2}}{\pi}\mathcal{I}m(A_\perp A_\parallel^*) . \tag{2.11}$$

Since the decay products identify the flavour at decay, the data can be separated into B^0 and $\overline{B}^0$ decays and the triple-product asymmetries calculated for both cases. This allows

JHEP05(2014)069

a determination of the *true* asymmetries, $A_T^k(\text{true}) = (A_T^k + \overline{A}_T^k)/2$, and so called *fake* asymmetries, $A_T^k(\text{fake}) = (A_T^k - \overline{A}_T^k)/2$, where $k = 1, 2$. In the Standard Model the value of $A_T^k(\text{true})$ is predicted to be zero and any deviation from this would indicate physics beyond the Standard Model. Non-zero values for $A_T^k(\text{fake})$ reflect the importance of strong final-state phases [4].

The S-wave contributions allow two additional triple-product asymmetries to be defined from h_9 and h_{13} in table 1,

$$\begin{aligned} A_T^3 &= \frac{\Gamma(s_{\theta_1}\sin\Phi > 0) - \Gamma(s_{\theta_1}\sin\Phi < 0)}{\Gamma(s_{\theta_1}\sin\Phi > 0) + \Gamma(s_{\theta_1}\sin\Phi < 0)} \\ &= -\sqrt{\frac{3}{2}}\int |M_1^{KK}(m_{KK})|^2 \mathcal{I}m(A_\perp A_{\rm S}^{*K\pi} M_1^{K\pi}(m_{K\pi}) M_0^{*K\pi}(m_{K\pi}))dm_{KK}dm_{K\pi}\,, \end{aligned} \tag{2.12}$$

and

$$\begin{aligned} A_T^4 &= \frac{\Gamma(s_{\theta_2}\sin\Phi > 0) - \Gamma(s_{\theta_2}\sin\Phi < 0)}{\Gamma(s_{\theta_2}\sin\Phi > 0) + \Gamma(s_{\theta_2}\sin\Phi < 0)} \\ &= -\sqrt{\frac{3}{2}}\int |M_1^{K\pi}(m_{K\pi})|^2 \mathcal{I}m(A_\perp A_{\rm S}^{*KK} M_1^{KK}(m_{KK}) M_0^{*KK}(m_{KK}))dm_{KK}dm_{K\pi}\,, \end{aligned} \tag{2.13}$$

where $s_{\theta_i} = \text{sign}(\cos\theta_i)$ for $i = 1, 2$.

3 Detector and dataset

The LHCb detector [25] is a single-arm forward spectrometer covering the pseudorapidity range $2 < \eta < 5$, designed for the study of particles containing b or c quarks. The detector includes a high-precision tracking system consisting of a silicon-strip vertex detector surrounding the pp interaction region, a large-area silicon-strip detector located upstream of a dipole magnet with a bending power of about 4 Tm, and three stations of silicon-strip detectors and straw drift tubes placed downstream. The polarity of the dipole magnet is reversed at intervals corresponding to roughly $0.1\,\text{fb}^{-1}$ of collected data, in order to minimize systematic uncertainties associated with detector asymmetries. The combined tracking system provides a momentum measurement with relative uncertainty that varies from 0.4 % at 5 GeV/c to 0.6 % at 100 GeV/c, and impact parameter resolution of 20 µm for tracks with high transverse momentum ($p_{\rm T}$). Charged hadrons are identified using two ring-imaging Cherenkov detectors [26]. Photon, electron and hadron candidates are identified by a calorimeter system consisting of scintillating-pad and preshower detectors, an electromagnetic calorimeter and a hadronic calorimeter. Muons are identified by a system composed of alternating layers of iron and multiwire proportional chambers.

The trigger [27] consists of a hardware stage, based on information from the calorimeter and muon systems, followed by a software stage, which applies a full event reconstruction. In this analysis two categories of events that pass the hardware trigger stage are considered: those where the signal b-hadron products are used in the trigger decision (TOS) and those

JHEP05(2014)069

where the trigger decision is caused by other activity in the event (TIS) [27]. The software trigger requires a three-track secondary vertex with large transverse momenta of the tracks and a significant displacement from the primary pp interaction vertices (PVs). At least one track should have $p_{\rm T} > 1.7\,{\rm GeV}/c$ and $\chi^2_{\rm IP}$ with respect to any primary interaction greater than 16, where $\chi^2_{\rm IP}$ is defined as the difference in χ^2 of a given PV reconstructed with and without the considered track. A multivariate algorithm [28] is used for the identification of secondary vertices consistent with the decay of a b hadron.

Simulated data samples are used to correct for the detector acceptance and response. In the simulation, pp collisions are generated using Pythia 6.4 [29] with a specific LHCb configuration [30]. Decays of hadronic particles are described by EvtGen [31], in which final-state radiation is generated using Photos [32]. The interaction of the generated particles with the detector and its response are implemented using the Geant4 toolkit [33, 34] as described in ref. [35].

4 Event selection

The selection of events is divided into two parts. In the first step a loose selection is performed that retains the majority of signal events, whilst reducing the background by a large fraction. Following this, a multivariate method is used to further reduce the background.

The selection starts from well reconstructed charged particles with a $p_{\rm T} > 500$ MeV/c that traverse the entire spectrometer. Fake tracks, not associated to actual charged particles, are suppressed using the output of a neural network trained to discriminate between these and real particles [36]. Further background suppression is achieved by exploiting the fact that the products of b-hadron decays have a large impact parameter (IP) with respect to the nearest PV. The IP of each track with respect to any primary vertex is required to have a $\chi^2_{\rm IP} > 9$.

To select well-identified pions and kaons, the difference in the logarithms of the likelihood of the kaon hypothesis relative to the pion hypothesis ($\mathrm{DLL}_{K\pi}$) is provided using information from the ring-imaging Cherenkov detectors. The kaons that form the $\phi \to K^+K^-$ candidate are required to have $\mathrm{DLL}_{K\pi} > 0$. To reduce background from $\pi^+\pi^-$ pairs, a tighter requirement, $\mathrm{DLL}_{K\pi} > 2$, is applied to the kaon in the $K^+\pi^-$ pair. For the pion in the $K^+\pi^-$ pair the requirement is $\mathrm{DLL}_{K\pi} < 0$.

The resulting charged particles are combined to form ϕ and K^{*0} meson candidates. The invariant mass of the K^+K^- ($K^+\pi^-$) pair is required to be within $\pm 15\,{\rm MeV}/c^2$ ($\pm 150\,{\rm MeV}/c^2$) of the known mass of the ϕ (K^{*0}) meson [1]. Finally, the $p_{\rm T}$ of the ϕ and K^{*0} mesons should both be greater than $900\,{\rm MeV}/c$, and the fit of their two-track vertices should have a $\chi^2 < 9$.

Candidate B^0 meson decays with $K^+K^-K^+\pi^-$ invariant mass in the range $5150 < m_{KKK\pi} < 5600\,{\rm MeV}/c^2$ are formed from pairs of selected ϕ and K^{*0} meson candidates. A fit is made requiring all four final-state particles to originate from a common vertex and the χ^2 per degree of freedom of this fit is required to be less than 15. To remove $B^0_s \to \phi\phi$ decays where a kaon has been incorrectly identified as a pion, the invariant mass of the $K^+\pi^-$ pair is recalculated assuming that both particles are kaons. If the resulting invariant mass

JHEP05(2014)069

is within $\pm 15\,\mathrm{MeV}/c^2$ of the known ϕ mass, the candidate is rejected. Finally, the decay vertex of the B^0 meson candidate is required to be displaced from the nearest PV, with a flight distance significance of more than 5 standard deviations, and the B^0 momentum vector is required to point back towards the PV with an impact parameter less than 0.3 mm and $\chi^2_{\rm IP} < 5$.

Further background suppression is achieved using a geometric likelihood (GL) method [15, 37, 38]. The GL is trained using a sample of simulated $B^0 \to \phi K^{*0}$ signal events together with background events selected from the upper mass sideband of the B^0 meson, $m_{KKK\pi} > 5413\,\mathrm{MeV}/c^2$, and the ϕ mass sidebands, $|m_{KK} - m_0^{\phi}| > 15\,\mathrm{MeV}/c^2$. These sidebands are not used in the subsequent analysis. Six discriminating variables are input to the GL: the IP of the B^0 candidate with respect to the PV, the distance of closest approach of the ϕ and K^{*0} meson candidate trajectories, the lifetime of the B^0 candidate, the transverse momentum of the B^0 candidate, the minimum $\chi^2_{\rm IP}$ of the K^+K^- pair and the minimum $\chi^2_{\rm IP}$ of the $K^+\pi^-$ pair. As a figure of merit the ratio $S/\sqrt{S+B}$ is considered, where S and B are the yields of signal and background events in the training samples, scaled to match the observed signal and background yields in the data. The maximum value for the figure of merit is found to be 24.6 for GL > 0.1, with signal and background efficiencies of 90 % and 21 %, respectively, compared to the selection performed without the GL. This reduces the sample size for the final analysis to 1852 candidates.

5 $K^+K^-K^+\pi^-$ mass model

The signal yield is determined by an unbinned maximum likelihood fit to the $K^+K^-K^+\pi^-$ invariant mass distribution. The selected mass range is chosen to avoid modelling partially reconstructed B decays with a missing hadron or photon. In the fit the signal invariant mass distribution is modelled as the sum of a Crystal Ball function [39] and a wider Gaussian function with a common mean. The width and fraction of the Gaussian function are fixed to values obtained using simulated events. A component is also included to account for the small contribution from the decay $\overline{B}{}^0_s \to \phi K^{*0}$ [38]. The shape parameters for this component are in common with the B^0 signal shape and the relative position of the B^0_s signal with respect to the B^0 signal is fixed using the known mass difference between B^0 and B^0_s mesons [1]. The invariant mass distribution is shown in figure 3, together with the result of the fit, from which a yield of 1655 ± 42 B^0 signal candidates is found.

After the selection the background is mainly combinatorial and is modelled by an exponential. Background from $B^0_s \to \phi\phi$ decays, with one of the kaons misidentified as a pion is reduced by the veto applied in the selection. The number of candidates from this source is estimated to be 6 events using simulation. These are distributed across the $K^+K^-K^+\pi^-$ mass range, and are considered negligible in the fit. A potential background from $B^0 \to D^+_s K^-(D^+_s \to \phi\pi^+)$ decays, which would peak in the signal region, is also found to be negligible. Possible background from the yet unobserved decay $\Lambda^0_b \to \phi p K^-$ with a misidentified proton is considered as part of the systematic uncertainties.

JHEP05(2014)069

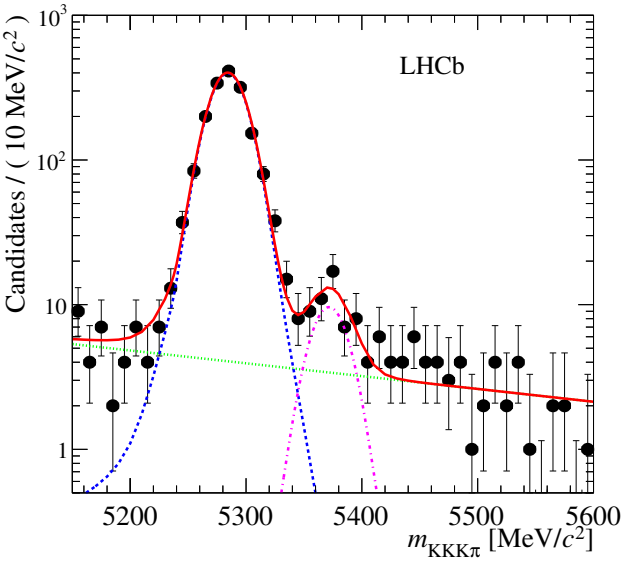

Figure 3. Invariant mass distribution for selected $K^+K^-K^+\pi^-$ candidates. A fit to the model described in the text is superimposed (red solid line). The signal contribution is shown as the blue dotted line. The contribution from combinatorial background is shown in green (dotted line). A contribution from $\overline{B}{}^0_s \to \phi K^{*0}$ (purple dot-dashed line) decays is visible around the known B^0_s meson mass.

6 Angular fit

The physics parameters of interest for this analysis are defined in table 2. They include the polarization amplitudes, phases and amplitude differences between B^0 and $\overline{B}{}^0$ decays from which the triple-product asymmetries are calculated.

The correlation between the fit variables and $m_{KKK\pi}$ is found to be less than 3 %. Therefore, the background can be subtracted using the *sPlot* method [40], with $m_{K^+K^-K^+\pi^-}$ as the discriminating variable. The results of the invariant mass fit discussed in section 5 are used to give each candidate a signal weight, W_n, which is a function of $m_{K^+K^-K^+\pi^-}$. The weight is used to subtract the background contributions from the distributions of the decay angles and intermediate resonance masses, which are fit using a signal-only likelihood that is a function of $\theta_1, \theta_2, \Phi, m_{K\pi}$ and m_{KK}. The angular fit minimizes the negative log likelihood summed over the n selected candidates

$$-\ln\mathcal{L} = -\alpha \sum_n W_n \ln\mathcal{S}_n \ , \tag{6.1}$$

where $\alpha = \sum_n W_n / \sum_n W_n^2$ is a normalization factor that includes the effect of the weights in the determination of the uncertainties [41, 42], and $\mathcal{S}$ is the signal probability density function (eq. (2.3)) convolved with the detector acceptance.

The acceptance of the detector is not uniform as a function of the decay angle of the $K^+\pi^-$ system (θ_1) and the $K^+\pi^-$ invariant mass. This is due to the 500 MeV/c criterion applied on the p_{T} of the pion from the K^{*0} meson decay. In contrast, the acceptance is

JHEP05(2014)069

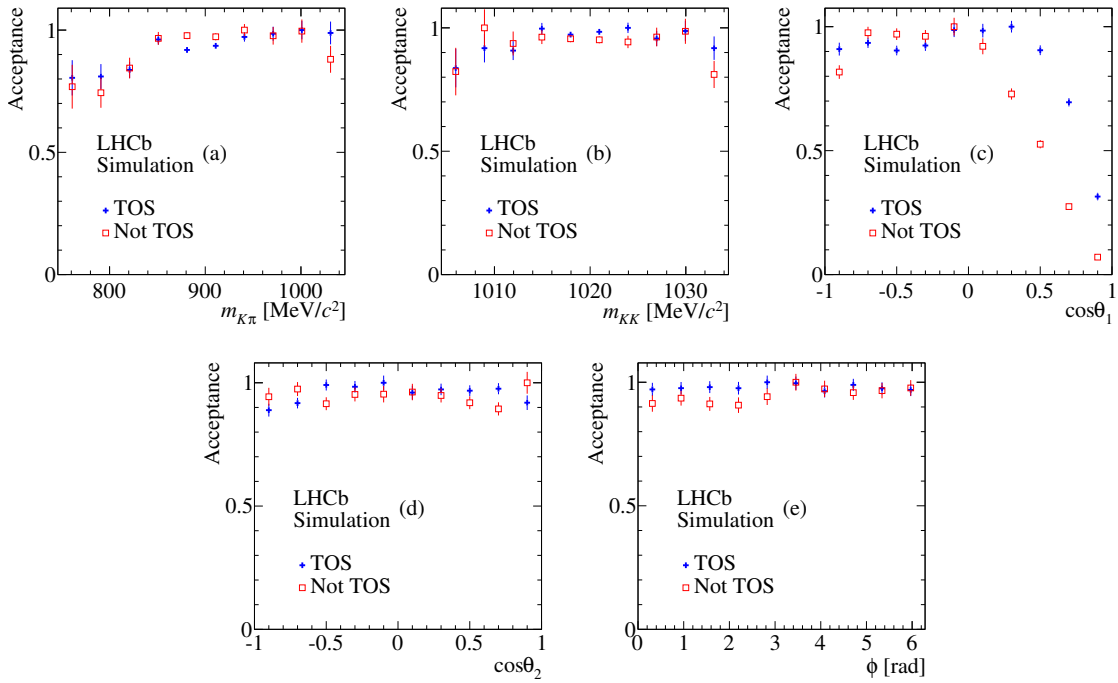

Figure 4. Binned projections of the detector acceptance for (a) $m_{K\pi}$, (b) m_{KK} , (c) $\cos\theta_1$, (d) $\cos\theta_2$ and (e) Φ. The acceptance for the TOS (filled crosses) and not TOS (open squares) are shown on each plot.

relatively uniform as a function of the decay angles θ_2 and Φ, and the invariant mass of the K^+K^- system.

The detector acceptance is modelled using a four-dimensional function that depends on the three decay angles and the $K^+\pi^-$ invariant mass. The shape of this function is obtained from simulated data. As the quantities relating to the $p_{\rm T}$ of the decay products are used in the first-level hardware based trigger, the acceptance is different for candidates that have a TIS or TOS decision at the hardware trigger stage [27]. Consequently, the trigger acceptance is calculated and corrected separately for the two categories. The 17 % of candidates that fall in the overlap between the two categories are treated as TOS, and the remaining TIS candidates are labelled 'not TOS'. The projections of the acceptance are shown in figure 4. In the subsequent analysis the data set is divided into the two categories and a simultaneous fit is performed.

7 Angular analysis results

Figure 5 shows the data distribution for the intermediate resonance masses and helicity angles with the projections of the best fit overlaid. The goodness of fit is estimated using a point-to-point dissimilarity test [43], the corresponding p-value is 0.64.

The fit results are listed in table 2. The value of f_L returned by the fit is close to 0.5, indicating that the longitudinal and transverse polarizations have similar size. Significant S-

JHEP05(2014)069

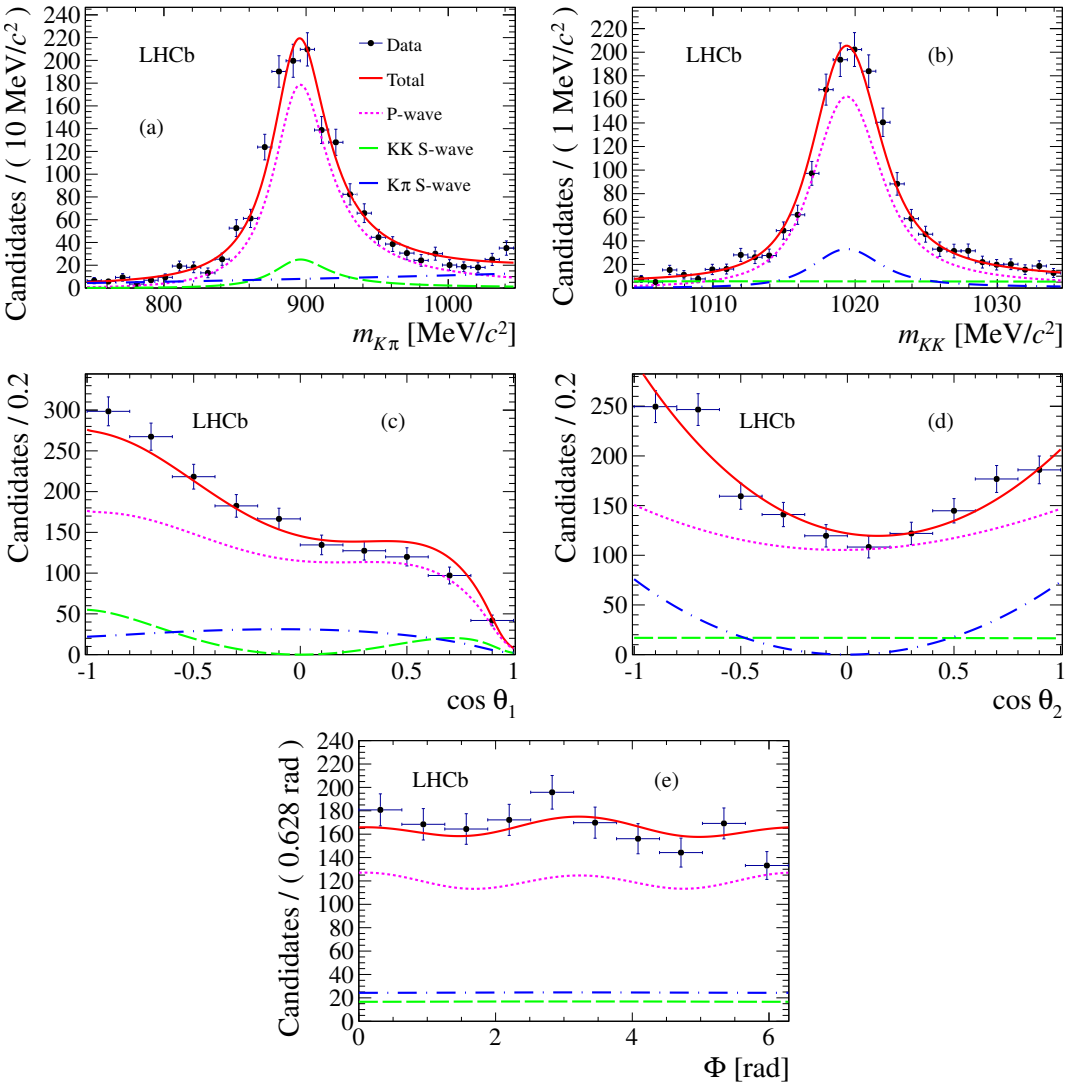

Figure 5. Data distribution for the helicity angles and of the intermediate resonance masses: (a) $m_{K\pi}$ and (b) m_{KK}, (c) $\cos\theta_1$, (d) $\cos\theta_2$ and (e) Φ. The background has been subtracted using the *sPlot* technique. The results of the fit are superimposed.

wave contributions are found in both the $K^+\pi^-$ and K^+K^- systems. The *CP* asymmetries in both the amplitudes and the phases are consistent with zero.

Using eqs. (2.11)–(2.13), the values for the triple-product asymmetries are derived from the measured parameters and given in table 3. The true asymmetries are consistent with zero, showing no evidence for physics beyond the Standard Model. In contrast, all but one of the fake asymmetries are significantly different from zero, indicating the presence of final-state interactions.

The systematic uncertainties on the measured amplitudes, phases and triple-product asymmetries are summarized in table 4. The largest systematic uncertainties on the results of the angular analysis arise from the understanding of the detector acceptance. The

JHEP05(2014)069

angular acceptance function is determined from simulated events as described in section 6. An uncertainty, labelled 'Acceptance' in the table, is assigned to account for the limited size of the simulation sample used. This is estimated using pseudo-experiments with a simplified simulation.

A difference is observed in the kinematic distributions of the final-state particles between data and simulation. This is attributed to the S-wave components, which are not included in the simulation. To account for this, the simulated events are reweighted to match the signal distributions as expected from the best estimate of the physics parameters from data (including the S-wave). In addition, the events are reweighted to match the observed distributions of the B^0 candidate and final-state particle transverse momenta. The reweighting is done separately for the two trigger categories and the nominal results are recalculated using the reweighted simulation to determine the angular acceptance. The difference between the weighted and unweighted results is taken as a systematic uncertainty (labelled 'Data/MC' in the table).

A further uncertainty arises from the $K^+K^-K^+\pi^-$ mass model used to determine the signal weights for the angular analysis. The fit procedure is repeated using different signal and background models. For the signal component a double Gaussian model is used instead of the sum of a Gaussian and a Crystal Ball function. Similarly, the influence of background modelling is probed using a first-order polynomial instead of an exponential function. Other changes to the background model are related to the possible presence of additional backgrounds. A possible small contribution from misidentified $\Lambda_b \to pK^-K^+K^-$ and $\Lambda_b \to p\pi^-K^+K^+$ decays is added and the fit repeated. Finally, the lower bound of the fit range is varied and the contribution from partially reconstructed B decays modelled. The largest difference compared to the central values is assigned as an estimate of the systematic uncertainty (labelled 'Mass model' in the table).

Alternative models of the S-wave contributions in both the K^+K^- and $K^+\pi^-$ system are considered. The default fit uses the LASS parameterization to model the $K^+\pi^-$ S-wave. As variations of this, both a pure phase-space model and a spin-0 relativistic Breit-Wigner with mean and width of the $K_0^*(1430)$ resonance are considered [1]. For the K^+K^- S-wave a pure phase-space model is tried in place of the Flatté parameterization. The largest observed deviation from the nominal fit is taken as a systematic uncertainty (column labelled 'S-wave' in the table).

Various consistency checks of the results are made. As a cross-check candidates that are in the overlap between the trigger categories are treated as TIS for the angular correction in the fit rather than TOS. The dataset is also divided according to the magnetic field polarity. The results obtained in these studies are consistent with the nominal results and no additional uncertainty is assigned.

8 Direct *CP* rate asymmetry

The raw measurement of the rate asymmetry is obtained from

$$A = \frac{N(\overline{B}^0 \to \phi\overline{K}^{*0}) - N(B^0 \to \phi K^{*0})}{N(\overline{B}^0 \to \phi\overline{K}^{*0}) + N(B^0 \to \phi K^{*0})} \,. \tag{8.1}$$

JHEP05(2014)069

Parameter	Definition	Fitted value
$f_{\rm L}$	$0.5(\lvert A_0\rvert^2/F_{\rm P} + \lvert\overline{A}_0\rvert^2/\overline{F}_{\rm P})$	$0.497 \pm 0.019 \pm 0.015$
$f_\perp$	$0.5(\lvert A_\perp\rvert^2/F_{\rm P} + \lvert\overline{A}_\perp\rvert^2/\overline{F}_{\rm P})$	$0.221 \pm 0.016 \pm 0.013$
$f_{\rm S}(K\pi)$	$0.5(\lvert A_{\rm S}^{K\pi}\rvert^2 + \lvert\overline{A}_{\rm S}^{K\pi}\rvert^2)$	$0.143 \pm 0.013 \pm 0.012$
$f_{\rm S}(KK)$	$0.5(\lvert A_{\rm S}^{KK}\rvert^2 + \lvert\overline{A}_{\rm S}^{KK}\rvert^2)$	$0.122 \pm 0.013 \pm 0.008$
$\delta_\perp$	$0.5(\arg A_\perp + \arg\overline{A}_\perp)$	$2.633 \pm 0.062 \pm 0.037$
$\delta_\parallel$	$0.5(\arg A_\parallel + \arg\overline{A}_\parallel)$	$2.562 \pm 0.069 \pm 0.040$
$\delta_{\rm S}(K\pi)$	$0.5(\arg A_{\rm S}^{K\pi} + \arg\overline{A}_{\rm S}^{K\pi})$	$2.222 \pm 0.063 \pm 0.081$
$\delta_{\rm S}(KK)$	$0.5(\arg A_{\rm S}^{KK} + \arg\overline{A}_{\rm S}^{KK})$	$2.481 \pm 0.072 \pm 0.048$
$\mathcal{A}_0^{CP}$	$(\lvert A_0\rvert^2/F_{\rm P} - \lvert\overline{A}_0\rvert^2/\overline{F}_{\rm P})/(\lvert A_0\rvert^2/F_{\rm P} + \lvert\overline{A}_0\rvert^2/\overline{F}_{\rm P})$	$-0.003 \pm 0.038 \pm 0.005$
$\mathcal{A}_\perp^{CP}$	$(\lvert A_\perp\rvert^2/F_{\rm P} - \lvert\overline{A}_\perp\rvert^2/\overline{F}_{\rm P})/(\lvert A_\perp\rvert^2/F_{\rm P} + \lvert\overline{A}_\perp\rvert^2/\overline{F}_{\rm P})$	$+0.047 \pm 0.074 \pm 0.009$
$\mathcal{A}_{\rm S}(K\pi)^{CP}$	$(\lvert A_{\rm S}^{K\pi}\rvert^2 - \lvert\overline{A}_{\rm S}^{K\pi}\rvert^2)/(\lvert A_{\rm S}^{K\pi}\rvert^2 + \lvert\overline{A}_{\rm S}^{K\pi}\rvert^2)$	$+0.073 \pm 0.091 \pm 0.035$
$\mathcal{A}_{\rm S}(KK)^{CP}$	$(\lvert A_{\rm S}^{KK}\rvert^2 - \lvert\overline{A}_{\rm S}^{KK}\rvert^2)/(\lvert A_{\rm S}^{KK}\rvert^2 + \lvert\overline{A}_{\rm S}^{KK}\rvert^2)$	$-0.209 \pm 0.105 \pm 0.012$
$\delta_\perp^{CP}$	$0.5(\arg A_\perp - \arg\overline{A}_\perp)$	$+0.062 \pm 0.062 \pm 0.005$
$\delta_\parallel^{CP}$	$0.5(\arg A_\parallel - \arg\overline{A}_\parallel)$	$+0.045 \pm 0.069 \pm 0.015$
$\delta_{\rm S}(K\pi)^{CP}$	$0.5(\arg A_{\rm S}^{K\pi} - \arg\overline{A}_{\rm S}^{K\pi})$	$+0.062 \pm 0.062 \pm 0.022$
$\delta_{\rm S}(KK)^{CP}$	$0.5(\arg A_{\rm S}^{KK} - \arg\overline{A}_{\rm S}^{KK})$	$+0.022 \pm 0.072 \pm 0.004$

Table 2. Parameters measured in the angular analysis. The first and second uncertainties are statistical and systematic, respectively.

Asymmetry	Measured value
A_T^1(true)	$-0.007 \pm 0.012 \pm 0.002$
A_T^2(true)	$+0.004 \pm 0.014 \pm 0.002$
A_T^3(true)	$+0.004 \pm 0.006 \pm 0.001$
A_T^4(true)	$+0.002 \pm 0.006 \pm 0.001$
A_T^1(fake)	$-0.105 \pm 0.012 \pm 0.006$
A_T^2(fake)	$-0.017 \pm 0.014 \pm 0.003$
A_T^3(fake)	$-0.063 \pm 0.006 \pm 0.005$
A_T^4(fake)	$-0.019 \pm 0.006 \pm 0.007$

Table 3. Triple-product asymmetries. The first and second uncertainties on the measured values are statistical and systematic, respectively.

The numbers of events, N, are determined from fits to the $m_{KKK\pi}$ invariant mass distribution performed separately for B^0 and $\overline{B}^0$ decays, identified using the charge of the final-state kaon. The dilution from the S-wave components is corrected for using the results of the angular analysis.

The candidates are separated into the TIS and TOS trigger categories. In this study, candidates that are accepted by both trigger decisions are included in both categories and

JHEP05(2014)069

Measurement	Acceptance	Data/MC	Mass model	S-wave	Total
$f_{\rm L}$	0.014	0.005	0.002	0.001	0.015
$f_\perp$	0.013	0.002	0.001	0.001	0.013
$f_{\rm S}(K\pi)$	0.012	—	0.001	0.002	0.012
$f_{\rm S}(KK)$	0.007	—	0.002	0.003	0.008
$\delta_\perp$	0.023	0.010	0.006	0.026	0.037
$\delta_\parallel$	0.029	0.013	0.004	0.024	0.040
$\delta_{\rm S}(K\pi)$	0.045	0.026	0.004	0.062	0.081
$\delta_{\rm S}(KK)$	0.045	0.005	0.004	0.016	0.048
$\mathcal{A}_0^{CP}$	—	0.002	0.002	0.004	0.005
$\mathcal{A}_\perp^{CP}$	—	0.001	0.006	0.007	0.009
$\mathcal{A}_{\rm S}(K\pi)^{CP}$	—	0.007	0.005	0.034	0.035
$\mathcal{A}_{\rm S}(KK)^{CP}$	—	0.007	0.009	0.003	0.012
$\delta_\perp^{CP}$	—	0.003	0.001	0.004	0.005
$\delta_\parallel^{CP}$	—	0.005	0.002	0.014	0.015
$\delta_{\rm S}(K\pi)^{CP}$	—	0.005	0.003	0.021	0.022
$\delta_{\rm S}(KK)^{CP}$	—	0.002	0.002	0.003	0.004
A_T^1(true)	—	0.0005	0.0005	0.002	0.002
A_T^2(true)	—	0.0006	0.0005	0.002	0.002
A_T^3(true)	—	0.0002	0.0003	0.001	0.001
A_T^4(true)	—	0.0002	0.0003	0.001	0.001
A_T^1(fake)	—	0.0019	0.0017	0.005	0.006
A_T^2(fake)	—	0.0008	0.0008	0.003	0.003
A_T^3(fake)	—	0.0015	0.0006	0.005	0.005
A_T^4(fake)	—	0.0003	0.0004	0.007	0.007

Table 4. Systematic uncertainties on the measurement of the polarization amplitudes, relative strong phases and triple-product asymmetries. The column labelled 'Total' is the quadratic sum of the individual contributions.

a possible bias to the central value is treated as a systematic uncertainty. The obtained raw asymmetries for the two trigger types are

$$A_{\phi K^{*0}}^{\rm TOS} = +0.014 \pm 0.043 \quad \text{and} \quad A_{\phi K^{*0}}^{\rm TIS} = -0.002 \pm 0.040 \,.$$

The direct *CP* asymmetry is related to the measured A by

$$A_{CP} = A - \delta \quad \text{with} \quad \delta = A_{\rm D} + \kappa_d A_{\rm P} \,, \tag{8.2}$$

where $A_{\rm D}$ is the detection asymmetry between $K^+\pi^-$ and $K^-\pi^+$ final-states, $A_{\rm P}$ is the asymmetry in production rate between B^0 and $\overline{B}^0$ mesons in pp collisions, and the factor κ_d accounts for the dilution of the production asymmetry due to $B^0 - \overline{B}^0$ oscillations.

The decay $B^0 \to J/\psi K^{*0}$ is used as a control channel to determine the difference in asymmetries

$$\Delta A_{CP} = A_{CP}(\phi K^{*0}) - A_{CP}(J/\psi K^{*0}) \,, \tag{8.3}$$

JHEP05(2014)069

Parameter	LHCb	BaBar	Belle
$f_{\rm L}$	$0.497 \pm 0.019 \pm 0.015$	$0.494 \pm 0.034 \pm 0.013$	$0.499 \pm 0.030 \pm 0.018$
$f_\perp$	$0.221 \pm 0.016 \pm 0.013$	$0.212 \pm 0.032 \pm 0.013$	$0.238 \pm 0.026 \pm 0.008$
$\delta_\perp$	$2.633 \pm 0.062 \pm 0.037$	$2.35 \pm 0.13 \pm 0.09$	$2.37 \pm 0.10 \pm 0.04$
$\delta_\parallel$	$2.562 \pm 0.069 \pm 0.040$	$2.40 \pm 0.13 \pm 0.08$	$2.23 \pm 0.10 \pm 0.02$
$\mathcal{A}_0^{CP}$	$-0.003 \pm 0.038 \pm 0.005$	$+0.01 \pm 0.07 \pm 0.02$	$-0.030 \pm 0.061 \pm 0.007$
$\mathcal{A}_\perp^{CP}$	$+0.047 \pm 0.072 \pm 0.009$	$-0.04 \pm 0.15 \pm 0.06$	$-0.14 \pm 0.11 \pm 0.01$
$\delta_\perp^{CP}$	$+0.062 \pm 0.062 \pm 0.006$	$+0.21 \pm 0.13 \pm 0.08$	$+0.05 \pm 0.10 \pm 0.02$
$\delta_\parallel^{CP}$	$+0.045 \pm 0.068 \pm 0.015$	$+0.22 \pm 0.12 \pm 0.08$	$-0.02 \pm 0.10 \pm 0.01$

Table 5. Comparison of measurements made by the LHCb, BaBar [8] and Belle [11] collaborations. The first uncertainty is statistical and the second systematic.

since the detector and production asymmetries cancel in the difference. Assuming A_{CP} to be zero for the tree-level $B^0 \to J/\psi K^{*0}$ decay, ΔA_{CP} is the *CP* asymmetry in $B^0 \to \phi K^{*0}$. The sample of $B^0 \to J/\psi K^{*0}$ decays, where the J/ψ meson decays to a muon pair, are collected through the same trigger and offline selections used for the signal decay mode. Candidates are placed in the TOS trigger category if the trigger decision is based on the decay products from the K^{*0} meson only. Where the decay products from the J/ψ meson influences the trigger decision, the candidate is rejected. The raw asymmetries obtained separately for the two trigger types are

$$A^{\rm TOS}_{J/\psi K^{*0}} = -0.003 \pm 0.016 \quad \text{and} \quad A^{\rm TIS}_{J/\psi K^{*0}} = -0.016 \pm 0.008 \,.$$

After averaging the trigger categories based on their statistical uncertainty, the measured value for the difference in *CP* asymmetries is

$$\Delta A_{CP} = (+1.5 \pm 3.2 \pm 0.5)\,\% \,,$$

where the uncertainties are statistical and systematic, respectively. Systematic uncertainties arise from the differences between the event topologies of the $B^0 \to J/\psi K^{*0}$ and $B^0 \to \phi K^{*0}$ decays. Differences in the behaviour of the events in the TIS trigger category between the signal and control modes lead to an uncertainty of 0.25 %. A further uncertainty of 0.4 % arises from the differences in kinematics of the daughter particles in the two modes. The double counting of candidates in the overlap region leads to a possible bias on the central value, estimated to be less than 0.1 %.

9 Conclusions

In this paper measurements of the polarization amplitudes and strong phase differences in the decay mode $B^0 \to \phi K^{*0}$ are reported. The results for the P-wave parameters are shown in table 5; these are consistent with, but more precise than previous measurements. All measurements are consistent with the presence of a large transverse component rather than the naïve expectation of a dominant longitudinal polarization.

JHEP05(2014)069

It is more difficult to make comparisons for the S-wave components as this is the first measurement to include consistently the effect of the S-wave in the K^+K^- system, and because the $K^+\pi^-$ mass range is different with respect to the range used in previous analyses. The measurements of the polarization amplitude differences are consistent with *CP* conservation.

The results of the angular analysis are used to determine triple-product asymmetries. The measured true asymmetries show no evidence for *CP* violation. In contrast, large fake asymmetries are observed, indicating the presence of significant final-state interactions. The difference in direct *CP* asymmetries between the $B^0 \to \phi K^{*0}$ and $B^0 \to J/\psi K^{*0}$ decays is also measured,

$$\Delta A_{CP} = (+1.5 \pm 3.2 \pm 0.5)\,\% \,,$$

where the first uncertainty is statistical and the second systematic. This is a factor of two more precise than previous values reported by BaBar and Belle [8, 11] and is found to be consistent with zero.

Acknowledgments

We express our gratitude to our colleagues in the CERN accelerator departments for the excellent performance of the LHC. We thank the technical and administrative staff at the LHCb institutes. We acknowledge support from CERN and from the national agencies: CAPES, CNPq, FAPERJ and FINEP (Brazil); NSFC (China); CNRS/IN2P3 and Region Auvergne (France); BMBF, DFG, HGF and MPG (Germany); SFI (Ireland); INFN (Italy); FOM and NWO (The Netherlands); SCSR (Poland); MEN/IFA (Romania); MinES, Rosatom, RFBR and NRC "Kurchatov Institute" (Russia); MinECo, XuntaGal and GENCAT (Spain); SNSF and SER (Switzerland); NASU (Ukraine); STFC (United Kingdom); NSF (USA). We also acknowledge the support received from EPLANET and the ERC under FP7. The Tier1 computing centres are supported by IN2P3 (France), KIT and BMBF (Germany), INFN (Italy), NWO and SURF (The Netherlands), PIC (Spain), GridPP (United Kingdom). We are indebted to the communities behind the multiple open source software packages on which we depend. We are also thankful for the computing resources and the access to software R&D tools provided by Yandex LLC (Russia).

References

[1] Particle Data Group, J. Beringer et al., *Review of particle physics*, *Phys. Rev.* **D 86** (2012) 010001 [INSPIRE].

[2] A. Datta and D. London, *Triple-product correlations in $B \to V_1 V_2$ decays and new physics*, *Int. J. Mod. Phys.* **A 19** (2004) 2505 [hep-ph/0303159] [INSPIRE].

JHEP05(2014)069

[3] D. London, N. Sinha and R. Sinha, *Bounds on new physics from $B \to V_1 V_2$ decays*, *Phys. Rev.* **D 69** (2004) 114013 [hep-ph/0402214] [INSPIRE].

[4] M. Gronau and J.L. Rosner, *Triple product asymmetries in K, $D_{(s)}$ and $B_{(s)}$ decays*, *Phys. Rev.* **D 84** (2011) 096013 [arXiv:1107.1232] [INSPIRE].

[5] CLEO collaboration, R.A. Briere et al., *Observation of $B \to \phi K$ and $B \to \phi K^*$*, *Phys. Rev. Lett.* **86** (2001) 3718 [hep-ex/0101032] [INSPIRE].

[6] BABAR collaboration, B. Aubert et al., *Measurement of the $B^0 \to \phi K^0$ decay amplitudes*, *Phys. Rev. Lett.* **93** (2004) 231804 [hep-ex/0408017] [INSPIRE].

[7] BABAR collaboration, B. Aubert et al., *Vector-tensor and vector-vector decay amplitude analysis of $B^0 \to \phi K^{*0}$*, *Phys. Rev. Lett.* **98** (2007) 051801 [hep-ex/0610073] [INSPIRE].

[8] BABAR collaboration, B. Aubert et al., *Time-dependent and time-integrated angular analysis of $B \to \phi K_s^0 \pi^0$ and $\varphi K_s^0 \pi^0$ and $\varphi K^{\pm} \pi^{\mp}$*, *Phys. Rev.* **D 78** (2008) 092008 [arXiv:0808.3586] [INSPIRE].

[9] BELLE collaboration, K. Chen et al., *Measurement of branching fractions and polarization in $B \to \phi K^{(*)}$ decays*, *Phys. Rev. Lett.* **91** (2003) 201801 [hep-ex/0307014] [INSPIRE].

[10] BELLE collaboration, K.-F. Chen et al., *Measurement of polarization and triple-product correlations in $B \to \phi K^*$ decays*, *Phys. Rev. Lett.* **94** (2005) 221804 [hep-ex/0503013] [INSPIRE].

[11] BELLE collaboration, M. Prim et al., *Angular analysis of $B^0 \to \phi K^*$ decays and search for CP-violation at Belle*, *Phys. Rev.* **D 88** (2013) 072004 [arXiv:1308.1830] [INSPIRE].

[12] BABAR collaboration, P. del Amo Sanchez et al., *Measurements of branching fractions, polarizations and direct CP-violation asymmetries in $B^+ \to \rho^0 K^{*+}$ and $B^+ \to f_0(980) K^{*+}$ decays*, *Phys. Rev.* **D 83** (2011) 051101 [arXiv:1012.4044] [INSPIRE].

[13] BELLE collaboration, J. Zhang et al., *Measurements of branching fractions and polarization in $B \to K^* \rho$ decays*, *Phys. Rev. Lett.* **95** (2005) 141801 [hep-ex/0408102] [INSPIRE].

[14] BABAR collaboration, B. Aubert et al., *Measurements of branching fractions, polarizations and direct CP-violation asymmetries in $B \to \rho K^*$ and $B \to f_0(980) K^*$ decays*, *Phys. Rev. Lett.* **97** (2006) 201801 [hep-ex/0607057] [INSPIRE].

[15] LHCb collaboration, *First observation of the decay $B_s^0 \to K^{*0} \bar{K}^{*0}$*, *Phys. Lett.* **B 709** (2012) 50 [arXiv:1111.4183] [INSPIRE].

[16] A.L. Kagan, *Polarization in $B \to VV$ decays*, *Phys. Lett.* **B 601** (2004) 151 [hep-ph/0405134] [INSPIRE].

[17] A. Datta, A.V. Gritsan, D. London, M. Nagashima and A. Szynkman, *Testing explanations of the $B \to \phi K^*$ polarization puzzle*, *Phys. Rev.* **D 76** (2007) 034015 [arXiv:0705.3915] [INSPIRE].

[18] P. Colangelo, F. De Fazio and Pham, *The riddle of polarization in $B \to VV$ transitions*, *Phys. Lett.* **B 597** (2004) 291 [hep-ph/0406162] [INSPIRE].

[19] M. Beneke, J. Rohrer and D. Yang, *Branching fractions, polarisation and asymmetries of $B \to VV$ decays*, *Nucl. Phys.* **B 774** (2007) 64 [hep-ph/0612290] [INSPIRE].

[20] H.-Y. Cheng and C.-K. Chua, *QCD factorization for charmless hadronic B_s decays revisited*, *Phys. Rev.* **D 80** (2009) 114026 [arXiv:0910.5237] [INSPIRE].

[21] D. Aston, N. Awaji, T. Bienz, F. Bird, J. D'Amore et al., *A study of $K^- \pi^+$ scattering in the reaction $K^- p \to K^- \pi^+ n$ at 11 GeV/c*, *Nucl. Phys.* **B 296** (1988) 493 [INSPIRE].

JHEP05(2014)069

[22] S.M. Flatte, *Coupled-channel analysis of the $\pi\eta$ and $K\bar{K}$ systems near $K\bar{K}$ threshold*, *Phys. Lett.* **B 63** (1976) 224 [INSPIRE].

[23] LHCb collaboration, *Analysis of the resonant components in $\overline{B}^0 \to J/\psi\pi^+\pi^-$*, *Phys. Rev.* **D 87** (2013) 052001 [arXiv:1301.5347] [INSPIRE].

[24] W. Bensalem and D. London, *T odd triple product correlations in hadronic b decays*, *Phys. Rev.* **D 64** (2001) 116003 [hep-ph/0005018] [INSPIRE].

[25] LHCb collaboration, *The LHCb detector at the LHC*, 2008 *JINST* **3** S08005 [INSPIRE].

[26] M. Adinolfi et. al., *Performance of the LHCb RICH detector at the LHC*, *Eur. Phys. J.* **C 73** (2013) 2431 [arXiv:1211.6759] [INSPIRE].

[27] R. Aaij et al., *The LHCb trigger and its performance in 2011*, 2013 *JINST* **8** P04022 [arXiv:1211.3055] [INSPIRE].

[28] V.V. Gligorov and M. Williams, *Efficient, reliable and fast high-level triggering using a bonsai boosted decision tree*, 2013 *JINST* **8** P02013 [arXiv:1210.6861] [INSPIRE].

[29] T. Sjöstrand, S. Mrenna and P.Z. Skands, *PYTHIA 6.4 physics and manual*, *JHEP* **05** (2006) 026 [hep-ph/0603175] [INSPIRE].

[30] I. Belyaev et al., *Handling of the generation of primary events in* Gauss, *the LHCb simulation framework*, *IEEE Nucl. Sci. Symp. Conf. Rec.* (2010) 1155.

[31] D. Lange, *The EvtGen particle decay simulation package*, *Nucl. Instrum. Meth.* **A 462** (2001) 152 [INSPIRE].

[32] P. Golonka and Z. Was, *PHOTOS Monte Carlo: a precision tool for QED corrections in Z and W decays*, *Eur. Phys. J.* **C 45** (2006) 97 [hep-ph/0506026] [INSPIRE].

[33] GEANT4 collaboration, J. Allison et al., *GEANT4 developments and applications*, *IEEE Trans. Nucl. Sci.* **53** (2006) 270.

[34] GEANT4 collaboration, S. Agostinelli et al., *GEANT4 — a simulation toolkit*, *Nucl. Instrum. Meth.* **A 506** (2003) 250 [INSPIRE].

[35] M. Clemencic et al., *The LHCb simulation application, gauss: design, evolution and experience*, *J. Phys. Conf. Ser.* **331** (2011) 032023 [INSPIRE].

[36] LHCb collaboration, *Observation of $B_c^+ \to J/\psi D_s^+$ and $B_c^+ \to J/\psi D_s^{*+}$ decays*, *Phys. Rev.* **D 87** (2013) 112012 [arXiv:1304.4530] [INSPIRE].

[37] D. Karlen, *Using projections and correlations to approximate probability distributions*, *Comput. Phys.* **12** (1998) 380 [physics/9805018] [INSPIRE].

[38] LHCb collaboration, *First observation of the decay $B_s^0 \to \phi\bar{K}^{*0}$*, *JHEP* **11** (2013) 092 [arXiv:1306.2239] [INSPIRE].

[39] T. Skwarnicki, *A study of the radiative cascade transitions between the Υ' and Υ resonances*, Ph.D. thesis, Institute of Nuclear Physics, Krakow, Poland (1986) [DESY-F31-86-02].

[40] M. Pivk and F.R. Le Diberder, *SPlot: a statistical tool to unfold data distributions*, *Nucl. Instrum. Meth.* **A 555** (2005) 356 [physics/0402083] [INSPIRE].

[41] LHCb collaboration, *Measurement of the B^0–$\bar{B}^0$ oscillation frequency Δm_d with the decays $B^0 \to D^-\pi^+$ and $B^0 \to J\,\psi K^{*0}$*, *Phys. Lett.* **B 719** (2013) 318 [arXiv:1210.6750] [INSPIRE].

[42] W.T. Eadie et al., *Statistical methods in experimental physics*, North Holland, Amsterdam The Netherlands (1971).

[43] M. Williams, *How good are your fits? Unbinned multivariate goodness-of-fit tests in high energy physics*, 2010 *JINST* **5** P09004 [arXiv:1006.3019] [INSPIRE].

JHEP05(2014)069

The LHCb collaboration

R. Aaij[41], A. Abba[21,u], B. Adeva[37], M. Adinolfi[46], A. Affolder[52], Z. Ajaltouni[5], J. Albrecht[9], F. Alessio[38], M. Alexander[51], S. Ali[41], G. Alkhazov[30], P. Alvarez Cartelle[37], A.A. Alves Jr[25,38], S. Amato[2], S. Amerio[22], Y. Amhis[7], L. An[3], L. Anderlini[17,g], J. Anderson[40], R. Andreassen[57], M. Andreotti[16,f], J.E. Andrews[58], R.B. Appleby[54], O. Aquines Gutierrez[10], F. Archilli[38], A. Artamonov[35], M. Artuso[59], E. Aslanides[6], G. Auriemma[25,n], M. Baalouch[5], S. Bachmann[11], J.J. Back[48], A. Badalov[36], V. Balagura[31], W. Baldini[16], R.J. Barlow[54], C. Barschel[38], S. Barsuk[7], W. Barter[47], V. Batozskaya[28], Th. Bauer[41], A. Bay[39], J. Beddow[51], F. Bedeschi[23], I. Bediaga[1], S. Belogurov[31], K. Belous[35], I. Belyaev[31], E. Ben-Haim[8], G. Bencivenni[18], S. Benson[50], J. Benton[46], A. Berezhnoy[32], R. Bernet[40], M.-O. Bettler[47], M. van Beuzekom[41], A. Bien[11], S. Bifani[45], T. Bird[54], A. Bizzeti[17,i], P.M. Bjørnstad[54], T. Blake[48], F. Blanc[39], J. Blouw[10], S. Blusk[59], V. Bocci[25], A. Bondar[34], N. Bondar[30,38], W. Bonivento[15,38], S. Borghi[54], A. Borgia[59], M. Borsato[7], T.J.V. Bowcock[52], E. Bowen[40], C. Bozzi[16], T. Brambach[9], J. van den Brand[42], J. Bressieux[39], D. Brett[54], M. Britsch[10], T. Britton[59], N.H. Brook[46], H. Brown[52], A. Bursche[40], G. Busetto[22,q], J. Buytaert[38], S. Cadeddu[15], R. Calabrese[16,f], O. Callot[7], M. Calvi[20,k], M. Calvo Gomez[36,o], A. Camboni[36], P. Campana[18,38], D. Campora Perez[38], F. Caponio[21,u], A. Carbone[14,d], G. Carboni[24,l], R. Cardinale[19,38,j], A. Cardini[15], H. Carranza-Mejia[50], L. Carson[50], K. Carvalho Akiba[2], G. Casse[52], L. Cassina[20], L. Castillo Garcia[38], M. Cattaneo[38], Ch. Cauet[9], R. Cenci[58], M. Charles[8], Ph. Charpentier[38], S.-F. Cheung[55], N. Chiapolini[40], M. Chrzaszcz[40,26], K. Ciba[38], X. Cid Vidal[38], G. Ciezarek[53], P.E.L. Clarke[50], M. Clemencic[38], H.V. Cliff[47], J. Closier[38], C. Coca[29], V. Coco[38], J. Cogan[6], E. Cogneras[5], P. Collins[38], A. Comerma-Montells[36], A. Contu[15,38], A. Cook[46], M. Coombes[46], S. Coquereau[8], G. Corti[38], M. Corvo[16,f], I. Counts[56], B. Couturier[38], G.A. Cowan[50], D.C. Craik[48], M. Cruz Torres[60], S. Cunliffe[53], R. Currie[50], C. D'Ambrosio[38], J. Dalseno[46], P. David[8], P.N.Y. David[41], A. Davis[57], K. De Bruyn[41], S. De Capua[54], M. De Cian[11], J.M. De Miranda[1], L. De Paula[2], W. De Silva[57], P. De Simone[18], D. Decamp[4], M. Deckenhoff[9], L. Del Buono[8], N. Déléage[4], D. Derkach[55], O. Deschamps[5], F. Dettori[42], A. Di Canto[38], H. Dijkstra[38], S. Donleavy[52], F. Dordei[11], M. Dorigo[39], A. Dosil Suárez[37], D. Dossett[48], A. Dovbnya[43], F. Dupertuis[39], P. Durante[38], R. Dzhelyadin[35], A. Dziurda[26], A. Dzyuba[30], S. Easo[49], U. Egede[53], V. Egorychev[31], S. Eidelman[34], S. Eisenhardt[50], U. Eitschberger[9], R. Ekelhof[9], L. Eklund[51,38], I. El Rifai[5], Ch. Elsasser[40], S. Esen[11], T. Evans[55], A. Falabella[16,f], C. Färber[11], C. Farinelli[41], S. Farry[52], D. Ferguson[50], V. Fernandez Albor[37], F. Ferreira Rodrigues[1], M. Ferro-Luzzi[38], S. Filippov[33], M. Fiore[16,f], M. Fiorini[16,f], M. Firlej[27], C. Fitzpatrick[38], T. Fiutowski[27], M. Fontana[10], F. Fontanelli[19,j], R. Forty[38], O. Francisco[2], M. Frank[38], C. Frei[38], M. Frosini[17,38,g], J. Fu[21], E. Furfaro[24,l], A. Gallas Torreira[37], D. Galli[14,d], S. Gambetta[19,j], M. Gandelman[2], P. Gandini[59], Y. Gao[3], J. Garofoli[59], J. Garra Tico[47], L. Garrido[36], C. Gaspar[38], R. Gauld[55], L. Gavardi[9], E. Gersabeck[11], M. Gersabeck[54], T. Gershon[48], Ph. Ghez[4], A. Gianelle[22], S. Giani'[39], V. Gibson[47], L. Giubega[29], V.V. Gligorov[38], C. Göbel[60], D. Golubkov[31], A. Golutvin[53,31,38], A. Gomes[1,a], H. Gordon[38], C. Gotti[20], M. Grabalosa Gándara[5], R. Graciani Diaz[36], L.A. Granado Cardoso[38], E. Graugés[36], G. Graziani[17], A. Grecu[29], E. Greening[55], S. Gregson[47], P. Griffith[45], L. Grillo[11], O. Grünberg[62], B. Gui[59], E. Gushchin[33], Yu. Guz[35,38], T. Gys[38], C. Hadjivasiliou[59], G. Haefeli[39], C. Haen[38], S.C. Haines[47], S. Hall[53], B. Hamilton[58], T. Hampson[46], X. Han[11], S. Hansmann-Menzemer[11], N. Harnew[55], S.T. Harnew[46], J. Harrison[54], T. Hartmann[62], J. He[38], T. Head[38], V. Heijne[41], K. Hennessy[52], P. Henrard[5], L. Henry[8], J.A. Hernando Morata[37], E. van Herwijnen[38], M. Heß[62], A. Hicheur[1], D. Hill[55], M. Hoballah[5], C. Hombach[54], W. Hulsbergen[41], P. Hunt[55], N. Hussain[55], D. Hutchcroft[52], D. Hynds[51], M. Idzik[27], P. Ilten[56], R. Jacobsson[38], A. Jaeger[11], J. Jalocha[55], E. Jans[41], P. Jaton[39],

JHEP05(2014)069

A. Jawahery[58], M. Jezabek[26], F. Jing[3], M. John[55], D. Johnson[55], C.R. Jones[47], C. Joram[38], B. Jost[38], N. Jurik[59], M. Kaballo[9], S. Kandybei[43], W. Kanso[6], M. Karacson[38], T.M. Karbach[38], M. Kelsey[59], I.R. Kenyon[45], T. Ketel[42], B. Khanji[20], C. Khurewathanakul[39], S. Klaver[54], O. Kochebina[7], M. Kolpin[11], I. Komarov[39], R.F. Koopman[42], P. Koppenburg[41,38], M. Korolev[32], A. Kozlinskiy[41], L. Kravchuk[33], K. Kreplin[11], M. Kreps[48], G. Krocker[11], P. Krokovny[34], F. Kruse[9], M. Kucharczyk[20,26,38,k], V. Kudryavtsev[34], K. Kurek[28], T. Kvaratskheliya[31], V.N. La Thi[39], D. Lacarrere[38], G. Lafferty[54], A. Lai[15], D. Lambert[50], R.W. Lambert[42], E. Lanciotti[38], G. Lanfranchi[18], C. Langenbruch[38], B. Langhans[38], T. Latham[48], C. Lazzeroni[45], R. Le Gac[6], J. van Leerdam[41], J.-P. Lees[4], R. Lefèvre[5], A. Leflat[32], J. Lefrançois[7], S. Leo[23], O. Leroy[6], T. Lesiak[26], B. Leverington[11], Y. Li[3], M. Liles[52], R. Lindner[38], C. Linn[38], F. Lionetto[40], B. Liu[15], G. Liu[38], S. Lohn[38], I. Longstaff[51], I. Longstaff[51], J.H. Lopes[2], N. Lopez-March[39], P. Lowdon[40], H. Lu[3], D. Lucchesi[22,q], H. Luo[50], A. Lupato[22], E. Luppi[16,f], O. Lupton[55], F. Machefert[7], I.V. Machikhiliyan[31], F. Maciuc[29], O. Maev[30], S. Malde[55], G. Manca[15,e], G. Mancinelli[6], M. Manzali[16,f], J. Maratas[5], J.F. Marchand[4], U. Marconi[14], C. Marin Benito[36], P. Marino[23,s], R. Märki[39], J. Marks[11], G. Martellotti[25], A. Martens[8], A. Martín Sánchez[7], M. Martinelli[41], D. Martinez Santos[42], F. Martinez Vidal[64], D. Martins Tostes[2], A. Massafferri[1], R. Matev[38], Z. Mathe[38], C. Matteuzzi[20], A. Mazurov[16,38,f], M. McCann[53], J. McCarthy[45], A. McNab[54], R. McNulty[12], B. McSkelly[52], B. Meadows[57,55], F. Meier[9], M. Meissner[11], M. Merk[41], D.A. Milanes[8], M.-N. Minard[4], J. Molina Rodriguez[60], S. Monteil[5], D. Moran[54], M. Morandin[22], P. Morawski[26], A. Mordà[6], M.J. Morello[23,s], J. Moron[27], R. Mountain[59], F. Muheim[50], K. Müller[40], R. Muresan[29], B. Muster[39], P. Naik[46], T. Nakada[39], R. Nandakumar[49], I. Nasteva[1], M. Needham[50], N. Neri[21], S. Neubert[38], N. Neufeld[38], M. Neuner[11], A.D. Nguyen[39], T.D. Nguyen[39], C. Nguyen-Mau[39,p], M. Nicol[7], V. Niess[5], R. Niet[9], N. Nikitin[32], T. Nikodem[11], A. Novoselov[35], A. Oblakowska-Mucha[27], V. Obraztsov[35], S. Oggero[41], S. Ogilvy[51], O. Okhrimenko[44], R. Oldeman[15,e], G. Onderwater[65], M. Orlandea[29], J.M. Otalora Goicochea[2], P. Owen[53], A. Oyanguren[64], B.K. Pal[59], A. Palano[13,c], F. Palombo[21,t], M. Palutan[18], J. Panman[38], A. Papanestis[49,38], M. Pappagallo[51], C. Parkes[54], C.J. Parkinson[9], G. Passaleva[17], G.D. Patel[52], M. Patel[53], C. Patrignani[19,j], A. Pazos Alvarez[37], A. Pearce[54], A. Pellegrino[41], M. Pepe Altarelli[38], S. Perazzini[14,d], E. Perez Trigo[37], P. Perret[5], M. Perrin-Terrin[6], L. Pescatore[45], E. Pesen[66], K. Petridis[53], A. Petrolini[19,j], E. Picatoste Olloqui[36], B. Pietrzyk[4], T. Pilař[48], D. Pinci[25], A. Pistone[19], S. Playfer[50], M. Plo Casasus[37], F. Polci[8], A. Poluektov[48,34], E. Polycarpo[2], A. Popov[35], D. Popov[10], B. Popovici[29], C. Potterat[2], A. Powell[55], J. Prisciandaro[39], A. Pritchard[52], C. Prouve[46], V. Pugatch[44], A. Puig Navarro[39], G. Punzi[23,r], W. Qian[4], B. Rachwal[26], J.H. Rademacker[46], B. Rakotomiaramanana[39], M. Rama[18], M.S. Rangel[2], I. Raniuk[43], N. Rauschmayr[38], G. Raven[42], S. Reichert[54], M.M. Reid[48], A.C. dos Reis[1], S. Ricciardi[49], A. Richards[53], K. Rinnert[52], V. Rives Molina[36], D.A. Roa Romero[5], P. Robbe[7], A.B. Rodrigues[1], E. Rodrigues[54], P. Rodriguez Perez[54], S. Roiser[38], V. Romanovsky[35], A. Romero Vidal[37], M. Rotondo[22], J. Rouvinet[39], T. Ruf[38], F. Ruffini[23], H. Ruiz[36], P. Ruiz Valls[64], G. Sabatino[25,l], J.J. Saborido Silva[37], N. Sagidova[30], P. Sail[51], B. Saitta[15,e], V. Salustino Guimaraes[2], C. Sanchez Mayordomo[64], B. Sanmartin Sedes[37], R. Santacesaria[25], C. Santamarina Rios[37], E. Santovetti[24,l], M. Sapunov[6], A. Sarti[18,m], C. Satriano[25,n], A. Satta[24], M. Savrie[16,f], D. Savrina[31,32], M. Schiller[42], H. Schindler[38], M. Schlupp[9], M. Schmelling[10], B. Schmidt[38], O. Schneider[39], A. Schopper[38], M.-H. Schune[7], R. Schwemmer[38], B. Sciascia[18], A. Sciubba[25], M. Seco[37], A. Semennikov[31], K. Senderowska[27], I. Sepp[53], N. Serra[40], J. Serrano[6], L. Sestini[22], P. Seyfert[11], M. Shapkin[35], I. Shapoval[16,43,f], Y. Shcheglov[30], T. Shears[52], L. Shekhtman[34], V. Shevchenko[63], A. Shires[9], R. Silva Coutinho[48], G. Simi[22], M. Sirendi[47], N. Skidmore[46], T. Skwarnicki[59], N.A. Smith[52], E. Smith[55,49], E. Smith[53], J. Smith[47], M. Smith[54], H. Snoek[41],

JHEP05(2014)069

M.D. Sokoloff[57], F.J.P. Soler[51], F. Soomro[39], D. Souza[46], B. Souza De Paula[2], B. Spaan[9], A. Sparkes[50], F. Spinella[23], P. Spradlin[51], F. Stagni[38], S. Stahl[11], O. Steinkamp[40], O. Stenyakin[35], S. Stevenson[55], S. Stoica[29], S. Stone[59], B. Storaci[40], S. Stracka[23,38], M. Straticiuc[29], U. Straumann[40], R. Stroili[22], V.K. Subbiah[38], L. Sun[57], W. Sutcliffe[53], K. Swientek[27], S. Swientek[9], V. Syropoulos[42], M. Szczekowski[28], P. Szczypka[39,38], D. Szilard[2], T. Szumlak[27], S. T'Jampens[4], M. Teklishyn[7], G. Tellarini[16,f], E. Teodorescu[29], F. Teubert[38], C. Thomas[55], E. Thomas[38], J. van Tilburg[41], V. Tisserand[4], M. Tobin[39], S. Tolk[42], L. Tomassetti[16,f], D. Tonelli[38], S. Topp-Joergensen[55], N. Torr[55], E. Tournefier[4], S. Tourneur[39], M.T. Tran[39], M. Tresch[40], A. Tsaregorodtsev[6], P. Tsopelas[41], N. Tuning[41], M. Ubeda Garcia[38], A. Ukleja[28], A. Ustyuzhanin[63], U. Uwer[11], V. Vagnoni[14], G. Valenti[14], A. Vallier[7], R. Vazquez Gomez[18], P. Vazquez Regueiro[37], C. Vázquez Sierra[37], S. Vecchi[16], J.J. Velthuis[46], M. Veltri[17,h], G. Veneziano[39], M. Vesterinen[11], B. Viaud[7], D. Vieira[2], M. Vieites Diaz[37], X. Vilasis-Cardona[36,o], A. Vollhardt[40], D. Volyanskyy[10], D. Voong[46], A. Vorobyev[30], V. Vorobyev[34], C. Voß[62], H. Voss[10], J.A. de Vries[41], R. Waldi[62], C. Wallace[48], R. Wallace[12], J. Walsh[23], S. Wandernoth[11], J. Wang[59], D.R. Ward[47], N.K. Watson[45], A.D. Webber[54], D. Websdale[53], M. Whitehead[48], J. Wicht[38], D. Wiedner[11], G. Wilkinson[55], M.P. Williams[45], M. Williams[56], F.F. Wilson[49], J. Wimberley[58], J. Wishahi[9], W. Wislicki[28], M. Witek[26], G. Wormser[7], S.A. Wotton[47], S. Wright[47], S. Wu[3], K. Wyllie[38], Y. Xie[61], Z. Xing[59], Z. Xu[39], Z. Yang[3], X. Yuan[3], O. Yushchenko[35], M. Zangoli[14], M. Zavertyaev[10,b], F. Zhang[3], L. Zhang[59], W.C. Zhang[12], Y. Zhang[3], A. Zhelezov[11], A. Zhokhov[31], L. Zhong[3], A. Zvyagin[38]

[1] *Centro Brasileiro de Pesquisas Físicas (CBPF), Rio de Janeiro, Brazil*
[2] *Universidade Federal do Rio de Janeiro (UFRJ), Rio de Janeiro, Brazil*
[3] *Center for High Energy Physics, Tsinghua University, Beijing, China*
[4] *LAPP, Université de Savoie, CNRS/IN2P3, Annecy-Le-Vieux, France*
[5] *Clermont Université, Université Blaise Pascal, CNRS/IN2P3, LPC, Clermont-Ferrand, France*
[6] *CPPM, Aix-Marseille Université, CNRS/IN2P3, Marseille, France*
[7] *LAL, Université Paris-Sud, CNRS/IN2P3, Orsay, France*
[8] *LPNHE, Université Pierre et Marie Curie, Université Paris Diderot, CNRS/IN2P3, Paris, France*
[9] *Fakultät Physik, Technische Universität Dortmund, Dortmund, Germany*
[10] *Max-Planck-Institut für Kernphysik (MPIK), Heidelberg, Germany*
[11] *Physikalisches Institut, Ruprecht-Karls-Universität Heidelberg, Heidelberg, Germany*
[12] *School of Physics, University College Dublin, Dublin, Ireland*
[13] *Sezione INFN di Bari, Bari, Italy*
[14] *Sezione INFN di Bologna, Bologna, Italy*
[15] *Sezione INFN di Cagliari, Cagliari, Italy*
[16] *Sezione INFN di Ferrara, Ferrara, Italy*
[17] *Sezione INFN di Firenze, Firenze, Italy*
[18] *Laboratori Nazionali dell'INFN di Frascati, Frascati, Italy*
[19] *Sezione INFN di Genova, Genova, Italy*
[20] *Sezione INFN di Milano Bicocca, Milano, Italy*
[21] *Sezione INFN di Milano, Milano, Italy*
[22] *Sezione INFN di Padova, Padova, Italy*
[23] *Sezione INFN di Pisa, Pisa, Italy*
[24] *Sezione INFN di Roma Tor Vergata, Roma, Italy*
[25] *Sezione INFN di Roma La Sapienza, Roma, Italy*
[26] *Henryk Niewodniczanski Institute of Nuclear Physics Polish Academy of Sciences, Kraków, Poland*
[27] *AGH - University of Science and Technology, Faculty of Physics and Applied Computer Science, Kraków, Poland*
[28] *National Center for Nuclear Research (NCBJ), Warsaw, Poland*

JHEP05(2014)069

[29] Horia Hulubei National Institute of Physics and Nuclear Engineering, Bucharest-Magurele, Romania
[30] Petersburg Nuclear Physics Institute (PNPI), Gatchina, Russia
[31] Institute of Theoretical and Experimental Physics (ITEP), Moscow, Russia
[32] Institute of Nuclear Physics, Moscow State University (SINP MSU), Moscow, Russia
[33] Institute for Nuclear Research of the Russian Academy of Sciences (INR RAN), Moscow, Russia
[34] Budker Institute of Nuclear Physics (SB RAS) and Novosibirsk State University, Novosibirsk, Russia
[35] Institute for High Energy Physics (IHEP), Protvino, Russia
[36] Universitat de Barcelona, Barcelona, Spain
[37] Universidad de Santiago de Compostela, Santiago de Compostela, Spain
[38] European Organization for Nuclear Research (CERN), Geneva, Switzerland
[39] Ecole Polytechnique Fédérale de Lausanne (EPFL), Lausanne, Switzerland
[40] Physik-Institut, Universität Zürich, Zürich, Switzerland
[41] Nikhef National Institute for Subatomic Physics, Amsterdam, The Netherlands
[42] Nikhef National Institute for Subatomic Physics and VU University Amsterdam, Amsterdam, The Netherlands
[43] NSC Kharkiv Institute of Physics and Technology (NSC KIPT), Kharkiv, Ukraine
[44] Institute for Nuclear Research of the National Academy of Sciences (KINR), Kyiv, Ukraine
[45] University of Birmingham, Birmingham, United Kingdom
[46] H.H. Wills Physics Laboratory, University of Bristol, Bristol, United Kingdom
[47] Cavendish Laboratory, University of Cambridge, Cambridge, United Kingdom
[48] Department of Physics, University of Warwick, Coventry, United Kingdom
[49] STFC Rutherford Appleton Laboratory, Didcot, United Kingdom
[50] School of Physics and Astronomy, University of Edinburgh, Edinburgh, United Kingdom
[51] School of Physics and Astronomy, University of Glasgow, Glasgow, United Kingdom
[52] Oliver Lodge Laboratory, University of Liverpool, Liverpool, United Kingdom
[53] Imperial College London, London, United Kingdom
[54] School of Physics and Astronomy, University of Manchester, Manchester, United Kingdom
[55] Department of Physics, University of Oxford, Oxford, United Kingdom
[56] Massachusetts Institute of Technology, Cambridge, MA, United States
[57] University of Cincinnati, Cincinnati, OH, United States
[58] University of Maryland, College Park, MD, United States
[59] Syracuse University, Syracuse, NY, United States
[60] Pontifícia Universidade Católica do Rio de Janeiro (PUC-Rio), Rio de Janeiro, Brazil, associated to[2]
[61] Institute of Particle Physics, Central China Normal University, Wuhan, Hubei, China, associated to[3]
[62] Institut für Physik, Universität Rostock, Rostock, Germany, associated to[11]
[63] National Research Centre Kurchatov Institute, Moscow, Russia, associated to [31]
[64] Instituto de Fisica Corpuscular (IFIC), Universitat de Valencia-CSIC, Valencia, Spain, associated to[36]
[65] KVI - University of Groningen, Groningen, The Netherlands, associated to[41]
[66] Celal Bayar University, Manisa, Turkey, associated to[38]

[a] Universidade Federal do Triângulo Mineiro (UFTM), Uberaba-MG, Brazil
[b] P.N. Lebedev Physical Institute, Russian Academy of Science (LPI RAS), Moscow, Russia
[c] Università di Bari, Bari, Italy
[d] Università di Bologna, Bologna, Italy
[e] Università di Cagliari, Cagliari, Italy
[f] Università di Ferrara, Ferrara, Italy
[g] Università di Firenze, Firenze, Italy

JHEP05(2014)069

[h] Università di Urbino, Urbino, Italy
[i] Università di Modena e Reggio Emilia, Modena, Italy
[j] Università di Genova, Genova, Italy
[k] Università di Milano Bicocca, Milano, Italy
[l] Università di Roma Tor Vergata, Roma, Italy
[m] Università di Roma La Sapienza, Roma, Italy
[n] Università della Basilicata, Potenza, Italy
[o] LIFAELS, La Salle, Universitat Ramon Llull, Barcelona, Spain
[p] Hanoi University of Science, Hanoi, Viet Nam
[q] Università di Padova, Padova, Italy
[r] Università di Pisa, Pisa, Italy
[s] Scuola Normale Superiore, Pisa, Italy
[t] Università degli Studi di Milano, Milano, Italy
[u] Politecnico di Milano, Milano, Italy

JHEP05(2014)069